SI Appendix

SI Materials and Methods

Reagents. Akt inhibitor VIII, KU-0063794, GDC-0941, PI-103 and Y-27632 were obtained from Chemdea. KN-93, KN-62, PD-168393, PD-153035, ERK inhibitor, ERK inhibitor II, U0126, PF-4708671, DG2, Gö-6976, bisindolylmaleimide-1, okadaic acid, cantharidic acid, and H-1152 were obtained from Calbiochem (Merck). GSK-1120212 and MK-2206 were obtained from Selleckchem. Torin-1 was obtained from Axon Medchem. Human recombinant EGF (AF-100-15) and IGF-1 (100-11) were purchased from Peprotech.

Cell-lines. MCF7 cells (identity confirmed by genotyping analysis) were routinely maintained in DMEM (supplemented with 10% fetal-bovine serum and 100 $U.mL^{-1}$ penicillin/streptomycin) at 37^{o}C in a humidified atmosphere at 5% CO_2. Resistant MCF7 cell-lines, derived from the original parental cells, were obtained by gradually increasing the concentrations of GDC-0941 or KU-0063794 concentrations (starting at 100 nM up to a maximum of 1 µM) over a period of approximately six months. The resultant clones (MCF7-G1:G3 and MCF7-K1:K3) were then routinely maintained as above in the presence of either 1 µM GDC-0941 or KU-0063794 (in DMSO) for MCF7-G and MCF7-K cells, respectively.

Cell lysis and protein digestion. Cells were split and seeded at 4 x 10^5 $cells.plate^{-1}$, 72 hours prior to the experiment. The medium in each plate was replaced 24 hours prior to the experiment. Each experiment was performed in biological duplicate. For the network definition experiments, cells were treated with each of the inhibitors or vehicle (DMSO) for 1 hour (Table S1). For the growth factor stimulation experiments, cells were starved for 24h and were subsequently treated with either 50 $ng.mL^{-1}$ EGF or IGF for 0, 5, 10, 30, or 60 minutes. For the resistant cell-line experiments, no additional treatments were performed. For the rewiring experiments in the MCF7-P and –G1:3 cell-lines, cells were starved for 24h and subsequently treated with 50 $ng.mL^{-1}$ EGF for 0, 30, 60, or 120 minutes. Following the treatments, cells were washed three times with ice-cold phosphate-buffered saline supplemented with 1 mM Na_3VO_4 and 1 mM NaF, and lysed with urea lysis buffer [8M urea in 20 mM HEPES (pH 8.0), supplemented with 1 mM Na_3VO_4, 1 mM NaF, 1 mM $Na_2P_2H_2O_7$, and 1 mM β-glycerol phosphate]. Lysates were further homogenized by probe sonication (three 10s pulses) and insoluble material removed by centrifugation. Protein concentration was estimated using the Bradford or Smith assay. After normalizing each condition to a common protein concentration (250 or 500 µg), each sample was reduced and alkylated by sequential incubation with 10 mM dithiothreitol and 16.6 mM iodoacetamide for 30 min at room temperature, in the dark. For protein digestion, the urea concentration was reduced to 2M by the addition of 20 mM HEPES (pH 8.0). Immobilised tosyl-lysine chloromethyl ketone (TLCK)-trypsin [20 *p*-toluenesulfonyl-L-arginine methyl ester (TAME) $units.mg^{-1}$] was then added, and

samples incubated overnight at 37^{o}C. Trypsin beads were removed by centrifugation and the resultant peptide solutions desalted with 30 mg Oasis-HLB cartridges (Waters, Manchester, UK), using a vacuum manifold. Briefly, Oasis cartridges were conditioned with acetonitrile (ACN) and equilibrated with wash solution (0.1% TFA, 1% ACN). Peptides were loaded into the cartridges and washed with 1 mL wash solution. Finally, peptides were eluted with glycolic acid buffer 1 (1M glycolic acid, 5% TFA, 50% ACN). When analyzing total protein, aliquots of the parental and original resistant cell-line lysates were taken and processed as above with the exception that the samples were eluted from the OASIS cartridges with 60% ACN (40% H_2O), dried-down using a SpeedVac, and stored at -80^{o}C until further analysis.

Phosphopeptide enrichment. Phosphorylated peptides were enriched using TiO_2 (GL Sciences) similarly to that previously described (1, 2) with some modifications outlined in supplementary Methods. Briefly, peptide eluents were normalized with glycolic acid buffer 2 (1M glycolic acid, 5% TFA, 80% ACN) and incubated with 50 µL of TiO_2 (a 50% slurry in 1% TFA), for 5 min at room temperature. Beads were pelleted by centrifugation, 80% of the supernatant removed and stored on ice. The remaining solution was used to re-suspend the beads, and the beads packed into pre-washed, empty, PE-filtered spin-tips (Glygen, MD, USA) by centrifugation. Residual beads were re-suspended with a further glycolic acid buffer 2 and packed into the tips. The remaining peptide solution was removed from ice and washed over the packed TiO_2 beads by centrifugation. The packed tips were then sequentially washed with glycolic acid buffer 2, ammonium acetate buffer (100 mM ammonium acetate; 25% ACN), and 10% ACN, the latter being repeated in triplicate. Phosphopeptides were eluted by centrifugation with four sequential washes of 5% NH_4OH in 10% ACN. The resulting phosphopeptide solutions were snap-frozen, dried in a SpeedVac, and stored at -80^{o}C.

LC-MS/MS phosphoproteomics analysis. Dried phosphopeptide extracts were re-suspended in 20 µL of 0.1% TFA (5% ACN) containing 20 fmol.µL^{-1} enolase digest (Waters, Manchester, UK). For each technical replicate, 3.0 µL of each sample was loaded into a Dionex Ultimate nRSLC 3000 LC system (Thermo Fisher Scientific) coupled online to an LTQ-Orbitrap-Velos mass spectrometer (Thermo Fisher Scientific). The samples were separated on an 85 min linear gradient between 5 and 35% ACN on a Acclaim PepMap RSLC column (25 cm x 75 µm, 2 µm, 100 Å), and the top seven most intense multiply charged ions in each MS^1 scan were selected for collision-induced dissociation fragmentation (with multistage activation enabled). The resolution of the MS^1 was set to 30,000 FWHM. Each sample was run in triplicate.

LC-MS/MS proteomics analysis. Dried peptide extracts were re-suspended to a final concentration of 0.5 µg.µL^{-1} in 0.1% TFA, 3% ACN. For each technical replicate, 4.0 µL of each sample was loaded into the LC-MS/MS system described above. The samples were separated on a 120 minute linear gradient between 3 and 32% ACN, and the top ten most intense multiply charged ions in each MS^1 scan were selected

for collision-induced dissociation fragmentation. The resolution of the MS^1 was set to 30,000 FWHM. Each sample was run in duplicate.

Phosphopeptide identification and quantification. Peptide identification was performed by matching deisotoped, MS/MS data to the Uniprot-Swissprot human protein databases (October 2012 release, containing 20,233 entries), utilizing the Mascot server version 2.3. Mascot Distiller version 2 was used to generate peak lists in the mascot generic format. The samples were also searched against a scrambled version of the former database. Mass tolerances were set to 10 ppm and 600 mmu for the precursor and fragment ions respectively. For the phosphoproteomics experiments, allowed variable modifications were phospho-Ser, phospho-Thr, phospho-Tyr, pyro-Glu (N-terminal), and oxidation-Met. The identified phosphopeptides from each of the samples were collated, curated, and a false-discovery rate calculated (by comparison to the scrambled database) using in-house scripts. Unique phosphopeptides ions with FDR < 5% were then included in the subsequent analyses. Using these settings >95% of peptides had a probability of FDR <1% (Fig. S1). The databases from the growth factor and resistant cell-line experiments were merged with the original network discovery database to ensure addition of the identified activity markers. Peptide quantification was performed as described before by our group (1-4) and others (5, 6). Briefly, Pescal software (written in Python v2.7) was used to obtain peak heights of extracted ion chromatograms of each of the phosphopeptide ions in the database, across all of the samples being compared. The retention times of each phosphopeptide ion in each sample were predicted by aligning the enolase standard peptides spiked into each sample, using an in-house linear modeling algorithm, and the subsequent integration of chromatographic peaks obtained from extracted ion chromatograms for each phosphopeptide in each sample. This approach is similar to that reported for the alignment of retention times in multiplexed selected reaction monitoring experiments (7). The mass-to-charge (m/z) and retention time (t_R) tolerances were set to 7 ppm and 1.5 min, respectively. Proteomics data were processed as above; however, protein identity was inferred only for those possessing ≥ 2 peptides with Mascot peptide scores ≥ 20 and a Mascot protein score ≥ 60.

Statistical analysis and data visualization. Following quantile normalization of the data (8), robust statistical analysis to assess the magnitude and significance of phosphorylation changes was performed using a linear modeling strategy and empirical Bayes shrinkage of standard deviations (9). The resulting *P*-values were then corrected for multiple testing using the Benjamini-Hochberg procedure. All of the described analysis was performed using the *limma* package (v3.16.2) within the R statistical computing environment (v3.0.0) (10, 11). The datasets were visualized using a combination of individual R packages, namely: *ggplot2*, *gplots*, *reshape2, igraph*, and *RCytoscape,* (12-16). Network graphs were constructed within the Cytoscape software package (v2.8.3) (17) and randomized using the *BiRewire* R package (18). Log_2 stoichiometry fold-ratios were calculated by subtracting the

calculated $\log_2$ ratio (vs control) of the total protein from the $\log_2$ fold-ratio (vs control) of the individual phosphorylation site.

Kinase-substrate enrichment analysis and motif analysis. The abundance of each of the identified markers was monitored systematically using KSEA (kinase-substrate enrichment analysis), as described previously (1). Briefly, the phosphopeptide ions identified within the growth factor and resistant cell-line experiments that were previously identified as being CTAMs were systematically extracted from the dataset. The mean of the $\log_2$ fold-ratios (versus control) of the phosphorylation sites representing each CTAM group were then calculated alongside the standard deviation (δ) for each mean. The significance of enrichment was then determined using a Z-score based approach and expressed as *P*-values, using the following formula: $Z = (S_m - \mu_t).m^{1/2}/\delta_t$; where S_m = mean of the CTAM group $\log_2$ fold-ratios; μ_t = mean of the total dataset $\log_2$ ratios; m = number of individual phosphopeptides within the CTAM group; and δ_t = standard deviation of the total dataset $\log_2$ ratios (vs control) (19). The motif analyses were performed as in (1). Briefly, the phosphopeptides under investigation were first grouped according to which consensus/common motif they represent. The mean $\log_2$ fold-ratio (vs DMSO control) was then calculated for each motif group under each condition.

CTAM identification algorithm. Phosphorylation sites were first filtered to only include those possessing a Mascot δ-score ≥ 5. Activity markers for each kinase inhibitor were then identified by selecting phosphorylation sites with a $\log_2$ fold-ratio ≤ 1 (i.e. a 50% linear reduction in abundance) and adjusted $P \leq 0.1$, or with those with a smaller change ($\log_2$ fold-ratio ≤ 0.75), but greater significance (adjusted $P \leq 0.05$) for each inhibitor. Phosphorylation sites that met the above thresholds under both inhibitor treatments targeting the same kinase were subsequently identified as compound-target activity markers (CTAMs).

Cell viability assays. Parental MCF7, G1:3 and K1:3 cell-lines were seeded in 96-well plates at a density of approximately 5,000 cells.well^{-1}, in biological triplicate. After 24 hours, the cells were then treated with the indicated concentrations/combinations of GDC-0941, KU-0063794, MK-2206, KN-93, PD-153035, GSK-1120212 or DMSO (as Table S2). Following a 48 hour treatment with the inhibitors, cell proliferation was determined with the MTS assay (Promega, WI, USA) or crystal violet stain. For the MTS assays the absorbance (490 nm) of each well was determined using a spectrophotometer following a 120 min incubation with the reagent, this measurement being acquired in duplicate. For the crystal violet staining, cells were fixed with 100 µL.well^{-1} paraformaldehyde (4% w/v in PBS) for 30 min on ice, stained with 100 µL.well^{-1} crystal violet stain (0.5% w/v in 20% MeOH) for 10 min at room temperature and washed twice with ddH_2O. Following the washes, the crystal violet was re-suspended using 100 µL.well^{-1} Sorensen's buffer (0.1M sodium citrate, 50% EtOH, pH 4.2) and the absorbance (540 nm) of each well measured in duplicate. The ratio of the absorbance of each concentration data-point

versus the absorbance of control (DMSO) treated cells was then calculated, log-transformed, and the mean of the each set of replicates calculated.

Cell proliferation assays. Parental MCF7, G1:3 and K1:3 cell-lines were seeded in 12-well plates at a density of approximately 80,000 cells.well^{-1}, in biological triplicate. After the indicated time period, cells were washed with PBS, trypsinized and counted using a Beckman Coulter Vi-CELL XR cell counter. Second-order polynomials where fitted to the data using the *ggplot2* package (v0.9.3.1) within R (v3.0.0).

Immunoblotting. Cells were lysed in lysis buffer (50 mM Tris-HCl [pH 7.4], 1 mM EDTA, 150 mM NaCl, 1% Triton-X100; supplemented with 1 mM Na_3VO_4, 1 mM NaF, 1 mM β-glycerol phosphate, 2.5 mM $Na_2P_2H_2O_7$, 1 mM PMSF, and 1X protease inhibitor cocktail [Sigma Aldrich]). Samples were resolved by SDS-polyacrylamide gel electrophoresis using either 12% or 4-15% gradient precast gels (BioRad). Proteins were transferred to PVDF membranes using the BioRad Trans-Blot Turbo system as per manufacturer's instructions. Once transferred, membranes were blocked with 5% w/v skimmed milk powder in Tris-buffered saline supplemented with 0.1% Tween-20. Blocked membranes were incubated with primary and secondary antibodies and developed with SuperSignal West Pico Chemiluminescent Substrate (Thermo Scientific). Primary antibodies (Table S4) were used at 1:500 or 1:1000 dilution and secondary antibodies were used at 1:5000 dilution.

Supplementary Figures

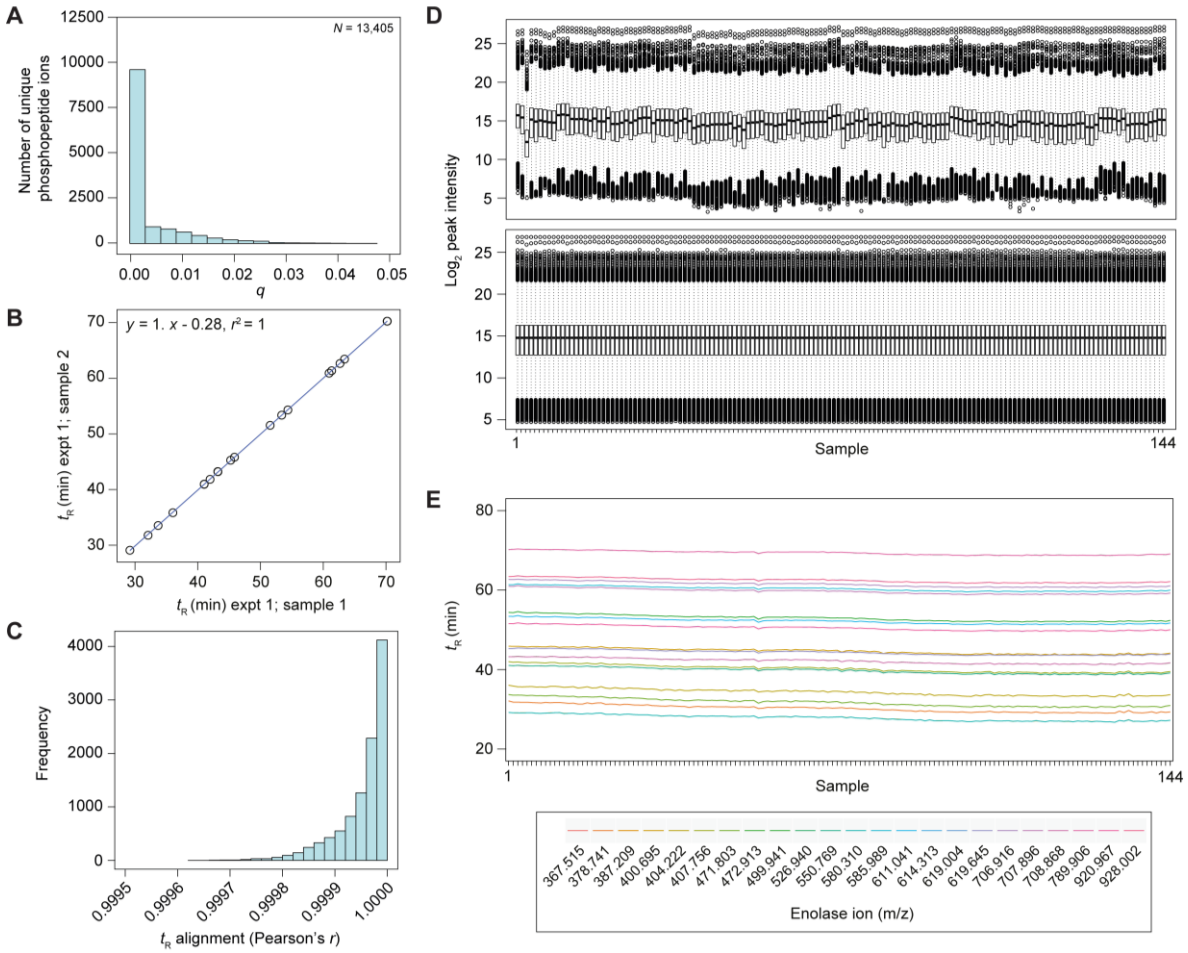

Fig. S1. Data summary for the kinase inhibitor-treated phosphoproteomes that define the network. This is a quality control analysis of the data shown in Fig. 1 and 2 in the main text. (A) Histogram showing the distribution of *q*-values within the phosphopeptide ion database (13,405 unique entries). (B) Box plots demonstrating the phosphopeptide ion $\log_2$ intensity distributions for each sample pre- (top panel) and post-quantile normalization (bottom panel). (C) Illustrative example of an enolase peptide standard retention time (t_R) alignment between two samples in order to predict and account for retention time shifts. (D) Histogram showing the distribution of Pearson's correlation coefficients (*r*) for linear models formed between each pair-wise peptide standard alignment. (E) Line plot demonstrating the stability of enolase peptide standard retention times across the sample array. The color of each line is specific to a single enolase peptide ion (as denoted in the key).

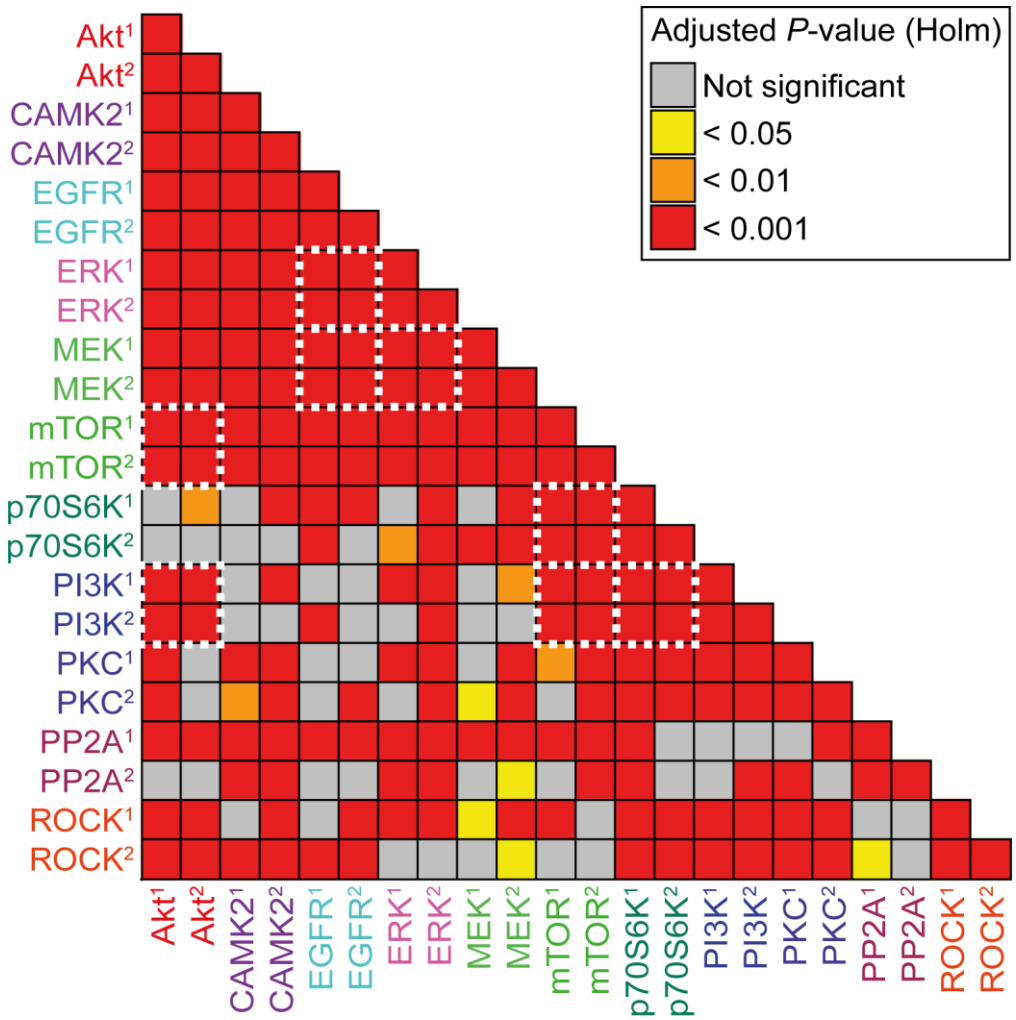

Fig. S2. Statistical significance of the correlations between inhibitor treatments. Heat map demonstrating the significance of correlation between each inhibitor treatment (based on the 4,651 phosphopeptide ions found to be significantly down-regulated by at least one inhibitor pair, as in Fig. 1C). The significance is expressed as an *P*-value (calculated from Pearson's *r* and adjusted for multiple testing using the Holm procedure) and color-coded accordingly. Known kinase-kinase relationships are highlighted with white, dashed boxes as in Fig. 1C.

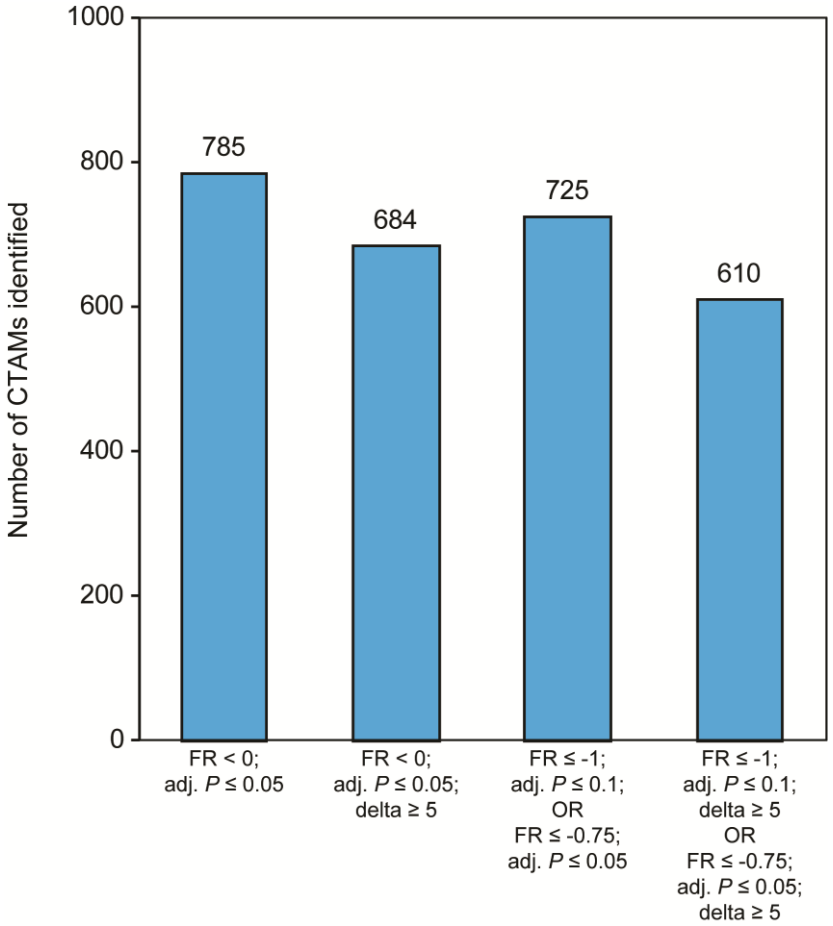

Fig. S3. Number of identified CTAMs as a function of selected statistical thresholds. Bars represent the number of CTAMs identified under the indicated threshold conditions. FR = $\log_2$ fold-ratio; adj. *P* = Benjamini-Hochberg adjusted *P*-value; delta = Mascot delta (δ) score.

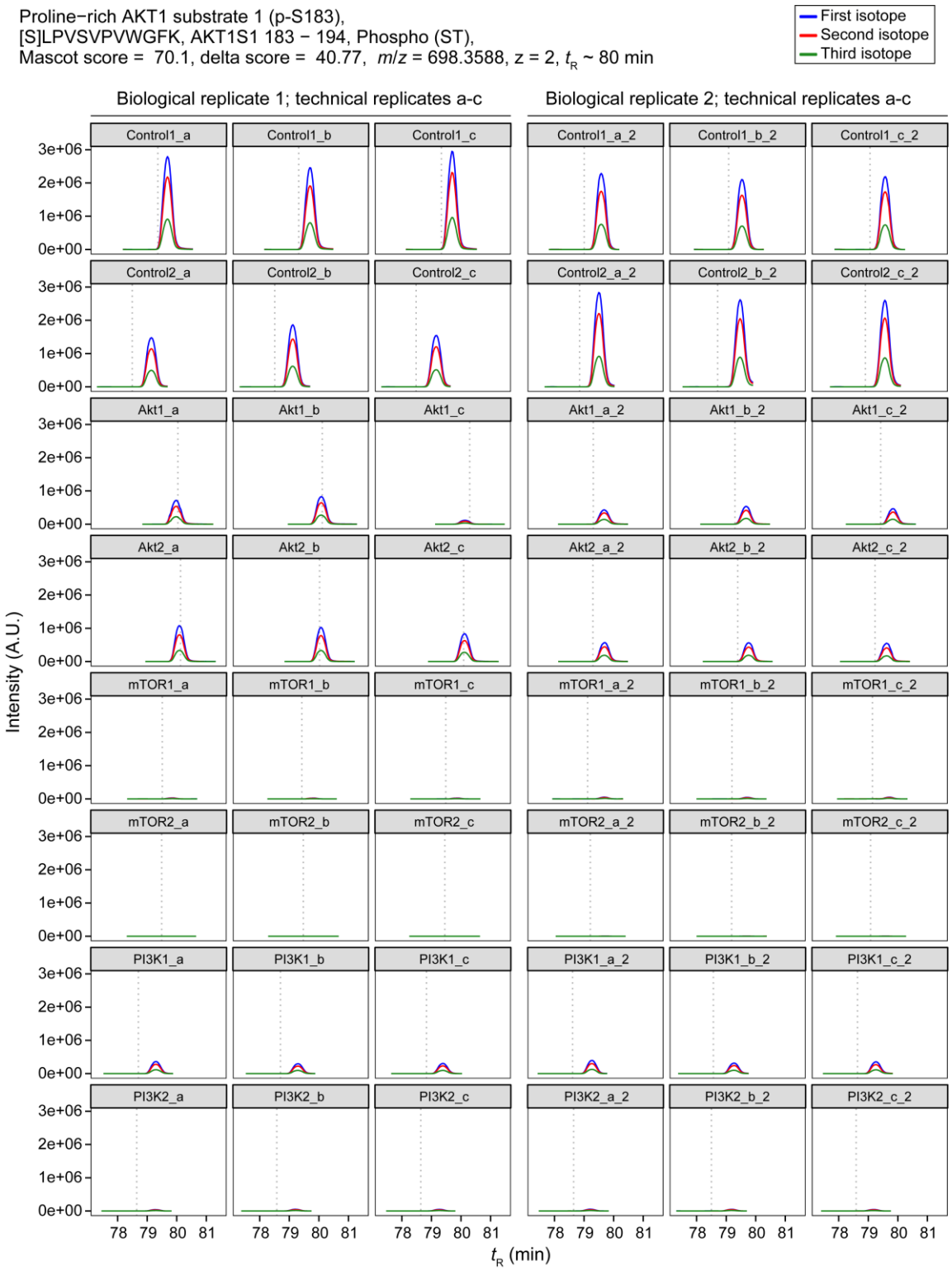

Fig. S4. Example of MS raw data. Raw MS data supports the identification of AKT1S as a member of the Akt-mTOR-PI3K CTAM group. Raw MS data extracted ion chromatograms (XICs) for the phosphopeptide representing AKT1S (S183) at *m/z* 698.3588 (± 7 ppm). Lines represent the temporal elution profiles of the first, second, and third isotopes as outlined in the key. Dotted lines represent the predicted retention time for the phosphopeptide in each sample. Akt1, Akt inhibitor VIII; Akt2, MK-2206; mTOR1, KU-0063794; mTOR2, Torin-1; PI3K1, GDC-0941; PI3K2, PI-103.

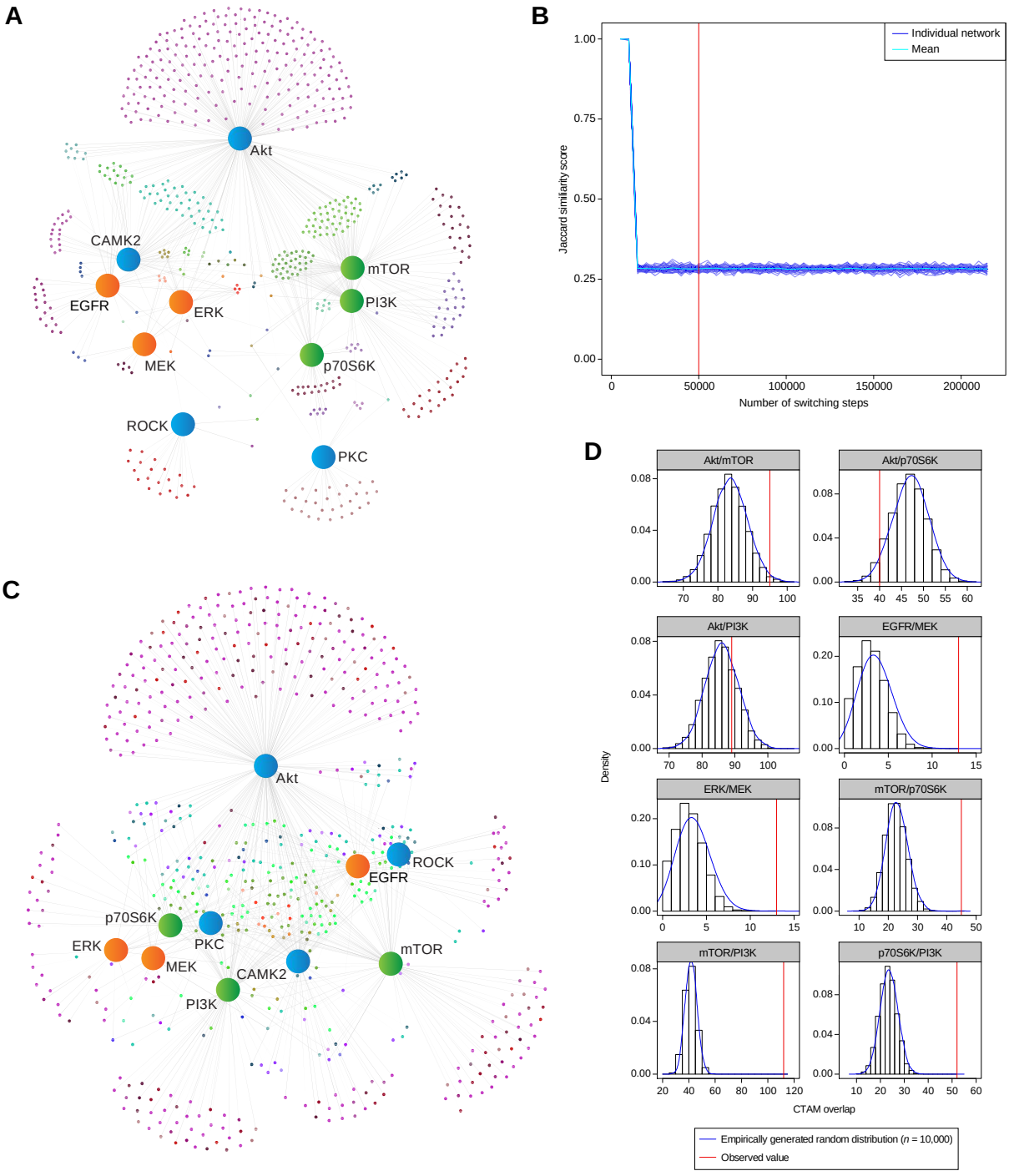

Fig. S5. Randomization of the defined network's topology. (A) Empirically defined kinase signaling network as shown in Fig. 2D. (B) Optimization of the number of switching steps required to produce networks least similar to the original. Red line, the number of switching steps used in subsequent network randomization attempts. (C) An illustrative example of one of the 10,000 randomized networks (produced using 50,000 switching steps). (D) Distribution of CTAM overlaps between the indicated kinases in the randomized networks. Blue line, probability density function of the overlaps observed in the 10,000 randomized networks (as in C); red line, overlap observed in the real network (as in A).

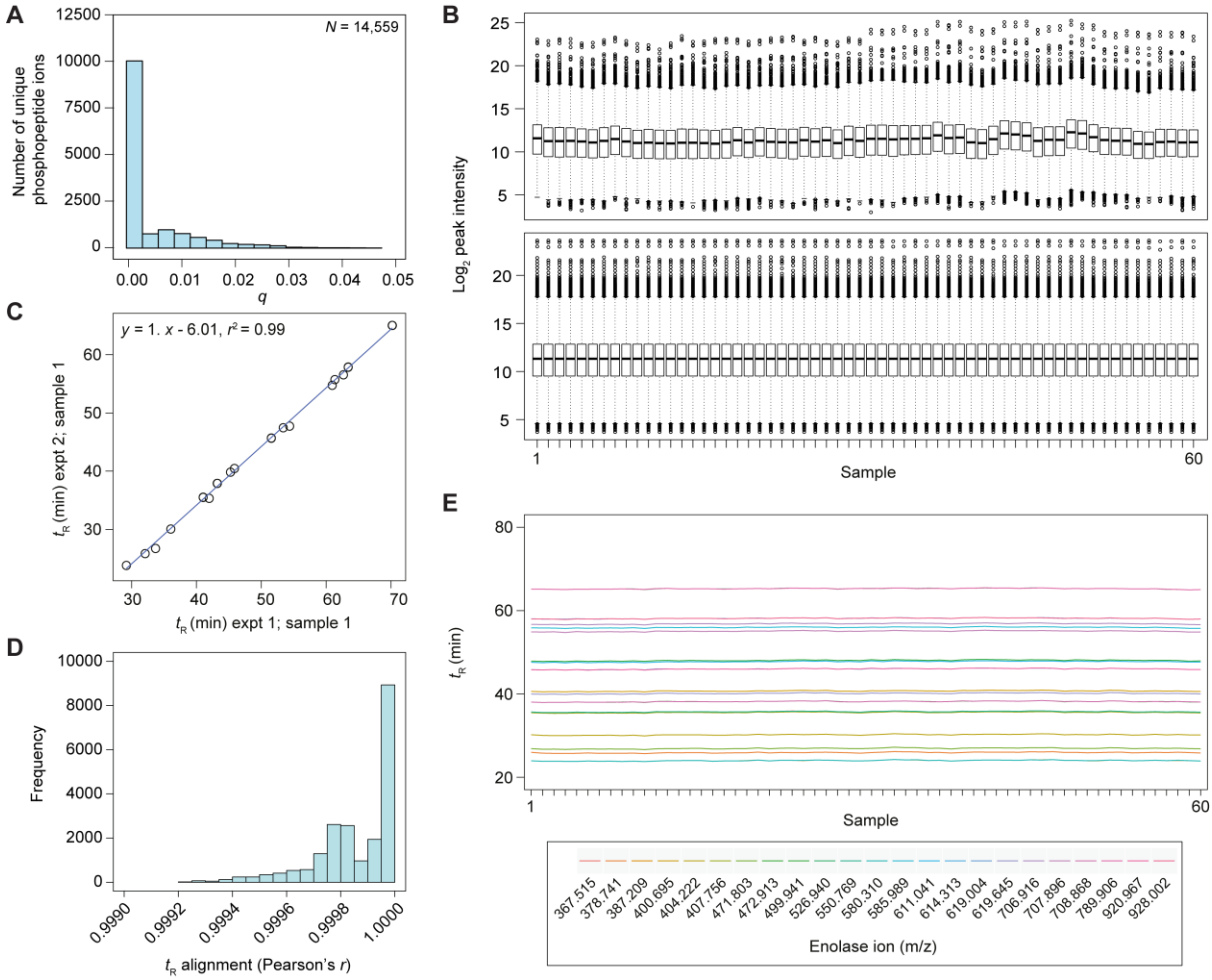

Fig. S6. Data summary for the stimulation of MCF7 cells with growth factors. This is a quality control analysis of the data shown in Fig. 3 in the main text. (A) Histogram showing the distribution of *q*-values within the phosphopeptide ion database (14,559 unique entries). (B) Box plots demonstrating the phosphopeptide ion $\log_2$ intensity distributions for each sample pre- (top panel) and post-quantile normalization (bottom panel). (C) Illustrative example of an enolase peptide standard retention time (t_R) alignment between two samples, one from the first, network-defining experiment (Fig S1 – expt 1) and one from the growth factor stimulation experiment (expt 2), in order to predict and account for retention time shifts. (D) Histogram showing the distribution of Pearson's correlation coefficients (*r*) for linear models formed between each pair-wise peptide standard alignment in both the network-defining and growth factor experiments. (E) Stability of enolase peptide standard retention times across the sample array. The color of each line is specific to a single enolase peptide ion (as denoted in the key).

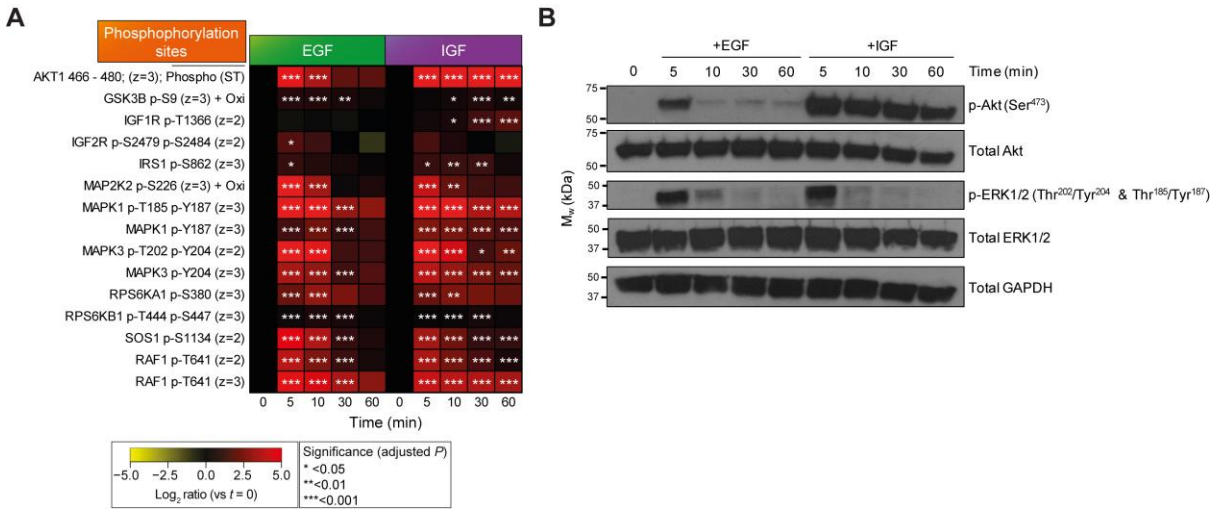

Fig. S7. Illustrative examples of the dynamics of phosphorylation sites downstream of EGFR and IGF-1R. Heat map showing the $\log_2$ fold-ratios (vs t = 0) for several phosphorylation sites known to be downstream of EGFR and IGF-1R following stimulation with either of the growth factors. Phosphorylation sites possessing a Mascot delta score ≥ 10 are presented as the protein name, peptide charge (z) ± any other peptide modifications. Those possessing a Mascot delta score ≤ 10 are represented as the protein name, residues between which the phosphorylation site resides, peptide charge, and the predicted modification. Asterisks indicate statistical significance (adjusted P-value) as outlined in the legend. (B) Western blots for known EGF/IGF-sensitive phosphorylation sites activating the Akt-mTOR-PI3K and MAPK pathways.

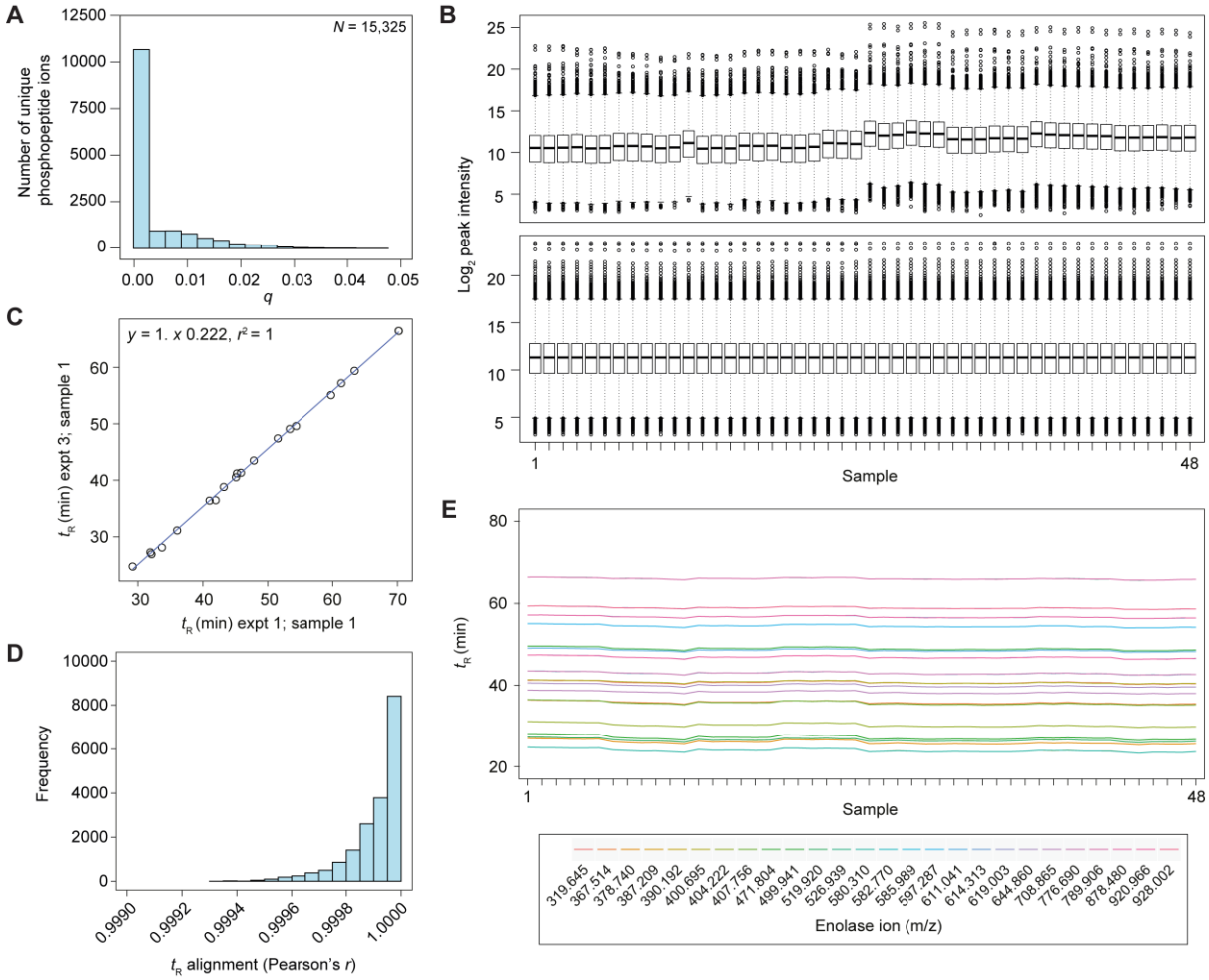

Fig. S8. Data summary for the quantitative phosphoproteomics comparison of resistant cell-lines and parental cells. This is a quality control analysis of the data shown in Fig. 4 in the main text. (A) Histogram showing the distribution of *q*-values within the phosphopeptide ion database (15,325 unique entries). (B) Box plots demonstrating the phosphopeptide ion $\log_2$ intensity distributions for each sample pre- (top panel) and post-quantile normalization (bottom panel). (C) Illustrative example of an enolase peptide standard retention time (t_R) alignment between two samples, one from the first, network-defining experiment (Fig S1 – expt 1) and one from the resistant cell-line comparison experiment (expt 3), in order to predict and account for retention time shifts. (D) Histogram showing the distribution of Pearson's correlation coefficients (*r*) for linear models formed between each pair-wise peptide standard alignment in both the network-defining and resistant cell-line experiments. (E) Stability of enolase peptide standard retention times across the sample array. The color of each line is specific to a single enolase peptide ion (as denoted in the key).

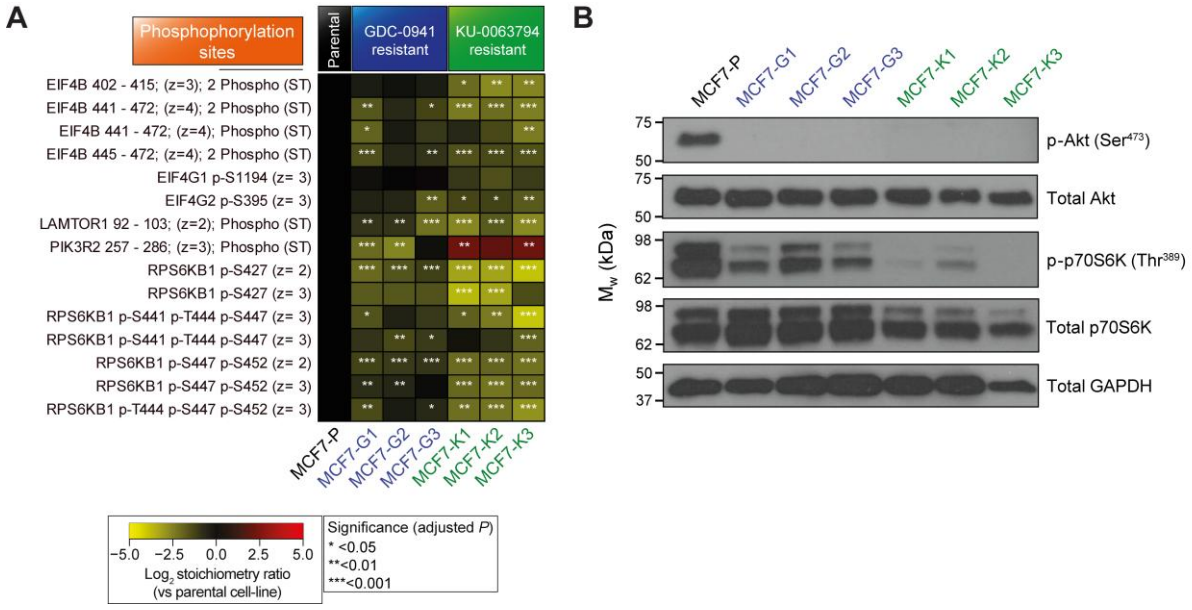

Fig. S9. Illustrative examples of phosphorylation sites reported to be downstream of PI3K and mTORC1/2 in resistant cell-lines treated with inhibitors. Heat map demonstrating the $\log_2$ stoichiometry ratios ($\log_2$ fold-ratio of the phosphorylation site/$\log_2$ fold-ratio of the protein) vs the parental cell-line of several phosphorylation sites known to be downstream of PI3K and mTORC1/2. Phosphorylation sites possessing a Mascot delta score ≥ 10 are presented as the protein name, peptide charge (*z*) ± any other peptide modifications. Those possessing a Mascot delta score ≤ 10 are represented as the protein name, residues between which the phosphorylation site resides, peptide charge, and the predicted modification. Asterisks indicate statistical significance (adjusted *P*-value) as outlined in the legend. (B) Western blots for known markers of Akt-mTOR-PI3K pathway activity.

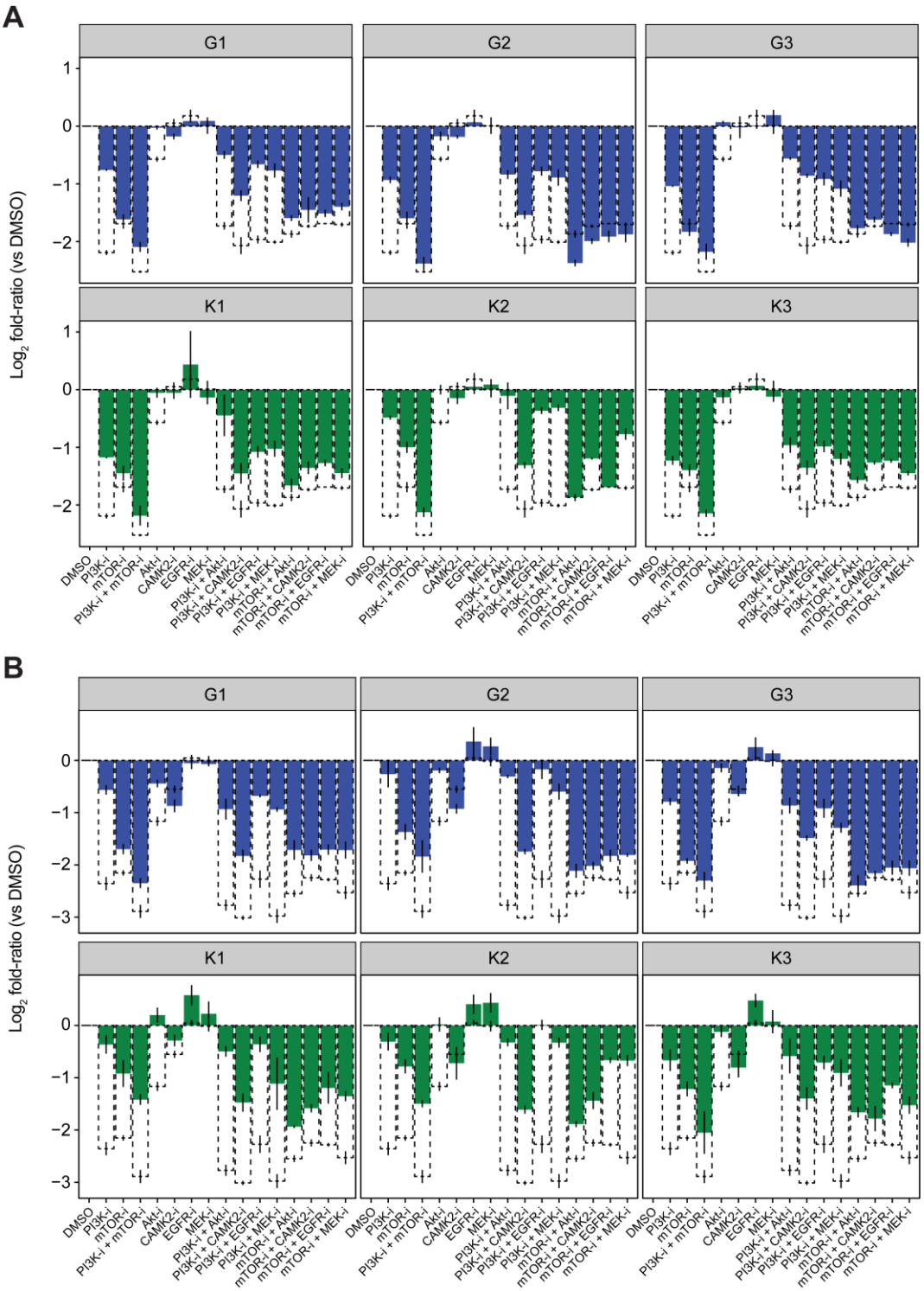

Fig. S10. Cell viability data for the resistant and parental cell-lines treated with a panel of kinase inhibitors. Bars represent mean $\log_2$ fold-ratio of cell viability (vs DMSO) for each kinase inhibitor alone or in combination in each of the resistant cell-lines (MCF7-G, solid blue; MCF7-K, solid green; MCF7-P, dotted white) as determined by the MTS assay. Error bars represent standard deviation from the mean in each case (*n* = 3). These data were the input for the PCA presented in Fig. 4E in the main text. PI3K-i = 1 μM GDC-0941; mTOR-i = 1 μM KU-0063794; Akt-i = 1 μM MK-2206; CAMK2-i = 5 μM KN-93; EGFR-i = 1 μM PD-153035; MEK-i = 0.5 μM GSK-1120212.

Table S1. Small-molecule inhibitors used in the experiments

Inhibitor	Concentration used (μM)	Primary target	Off-targets from MRC database (>50% inhibition at given concentration)	ChEMBL ID	Off-targets from ChEMBL	Reference material
Akt inhibitor VIII	1	Akt1/2/3	CAMK1 (1 μM)	258844	-	(20)
MK-2206	1	Akt1/2/3	-	1079175	-	(21, 22)
KN-62	5	CAMK2α/β/γ/δ	PRAK, CAMK1, DYRK1A, Lck (10 μM)	155333	P2RX7	(23)
KN-93	10	CAMK2α/β/γ/δ	TrkA, smMLCK (10 μM)	28234	-	(24)
PD-168393	1	EGFR	-	285063	ERBB2/4, BMX, BTK, BLK, JAK3	(25)
PD-153035	10	EGFR	-	29197	ABL1, ERBB2, MKNK1, F16P1	(26)
ERK inhibitor I	40	ERK1/2	-	1403932	-	(27)
ERK inhibitor II (FR180204)	30	ERK1/2	-	259551	MAPK14	(28)
GSK-1120212	0.5	MEK1/2	-	-	-	(29, 30)
U0126	10	MEK1/2	MKK1 (10 μM)	100473	-	(30, 31)
KU-0063794	1	mTORC1/2	-	1078983	-	(32)
Torin-1	1	mTORC1/2	-	1256459	PI3Kα/δ/γ, p85α, PI3K-C2α/β, Vps34, DNA-PK	(33)
PF-4708671	20	p70S6K (S6K1)	MSK1, RSK1 (1 μM)	-	S6Kα5	(34)
DG2	5	p70S6K (S6K1)	-	1254209	-	(35)
GDC-0941	1	PI3K (class I)	CLK2 (1 μM)	573393	Akt1, mTOR, HIPK2/3, MYLK4, CLK2, MAPK10, FLT3, JAK1, RIOK2	(36, 37)
PI-103	1	PI3K (class I)	-	521851	mTOR, DNA-PK, Akt1	(38)
Gö-6976	1	PKCα/β/δ/γ	MKK1, BRSK2, ERK2/8, CAMKKα, MNK2, DYRK1A/3, SmMLCK, HIPK2, Aurora C, GSK3β, Aurora B, PIM1, MELK, AMPK, MARK3, CAMKKβ, S6K1, PDK1, CDK2, RSK1, PAK4/5/6, MSK1, PKD1, PIM3, RSK2, PRK2, PHK, CHK1, MST2 (0.1 μM)	302449	PKD1	(39)
Bisindolylmaleimide-I	1	PKCα/θ/η/γ/ε	MKK1, ROCK2, Lck, PKA, Akt1, MAPKAP-K2, CHK1, PKD1, AMPK, S6K1, GSK3β, CDK2, SGK1, DYRK1A, MSK1, PHK, RSK1 (10 μM)	7463	CDK4/CCND1, GSK3β, PIM1	(40)
Okadaic acid	1	PP2A	-	280487	-	(41)
Cantharidic acid	10	PP2A	-	275516	-	(42)
H-1152	5	ROCK	MNK1, MARK3, MELK, EPH-A2, RSK2, MSK1, BRSK2, FGF-R1, PKA, AMPK, RSK1, PHK, Aurora B/C, PRK2 (1 μM)	406821	PKA	(43)
Y-27632	10	ROCK	PHK, MST2, RSK2, MSK1, MNK1, RSK1, AMPK, PRK2 (1 μM)	-	PKCε	(44)

Table S2. The identified CTAMs

CTAM group	Phosphorylation site
Akt-CAMK2-EGFR-ERK-MEK-mTOR	PHF12(S977)
Akt-CAMK2-EGFR-ERK-MEK-mTOR	PRCC(S267)
Akt-CAMK2-EGFR-ERK-MEK-mTOR	SERPINA10(T297)
Akt-CAMK2-EGFR-ERK-MEK-mTOR	SSFA2(S737+S739)
Akt-CAMK2-EGFR-ERK-MEK	EIF3G(T41+S42)
Akt-CAMK2-EGFR-ERK-MEK	JUND(S90)
Akt-CAMK2-EGFR-ERK-MEK	PBK(T24+S32)
Akt-CAMK2-EGFR-ERK-MEK	RPLP2(S102+S105)
Akt-CAMK2-EGFR-ERK-ROCK	ANXA13(Y291+S294)
Akt-CAMK2-ERK-MEK-mTOR	USP13(S630)
Akt-CAMK2-mTOR-p70S6K-PI3K	RICTOR(T1135+S1138)
Akt-ERK-mTOR-p70S6K-PI3K	ZNF687(S1118)
Akt-mTOR-p70S6K-PI3K-PKC	WWTR1(S93)
Akt-CAMK2-EGFR-ERK	DSP(S38)
Akt-CAMK2-EGFR-ERK	KAT7(T302+S303)
Akt-CAMK2-EGFR-ERK	KLF16(S230)
Akt-CAMK2-EGFR-ERK	NOS1AP(S371+S374)
Akt-CAMK2-EGFR-ERK	PER2(S77)
Akt-CAMK2-EGFR-ERK	TNKS1BP1(S494+S504)
Akt-CAMK2-EGFR-mTOR	PLEC(T4030)
Akt-CAMK2-EGFR-p70S6K	GAPDH(T184)
Akt-CAMK2-ERK-MEK	FBRSL1(T989+T1010)
Akt-CAMK2-mTOR-PI3K	EIF4EBP1(T41+S44)
Akt-EGFR-ERK-mTOR	DLGAP4(S973)
Akt-mTOR-p70S6K-PI3K	C10orf47(S43)
Akt-mTOR-p70S6K-PI3K	C2orf78(S624+S625)
Akt-mTOR-p70S6K-PI3K	CHD1(S1385)
Akt-mTOR-p70S6K-PI3K	CHD1(S1387)
Akt-mTOR-p70S6K-PI3K	CIC(S299)
Akt-mTOR-p70S6K-PI3K	CLMN(S921)
Akt-mTOR-p70S6K-PI3K	CNBP(S47)
Akt-mTOR-p70S6K-PI3K	CTDSPL2(S28)
Akt-mTOR-p70S6K-PI3K	EHMT2(S232)
Akt-mTOR-p70S6K-PI3K	EPRS(T956)
Akt-mTOR-p70S6K-PI3K	GTPBP4(T201+T202)
Akt-mTOR-p70S6K-PI3K	HMGCR(S872)
Akt-mTOR-p70S6K-PI3K	IFT122(Y146+S157)
Akt-mTOR-p70S6K-PI3K	KRT8(S477)
Akt-mTOR-p70S6K-PI3K	MACF1(S1376)
Akt-mTOR-p70S6K-PI3K	MACF1(S1378)
Akt-mTOR-p70S6K-PI3K	MTDH(S494)
Akt-mTOR-p70S6K-PI3K	MYO5A(S1652)
Akt-mTOR-p70S6K-PI3K	NEK9(S332)
Akt-mTOR-p70S6K-PI3K	NOLC1(S686+S698)
Akt-mTOR-p70S6K-PI3K	PCBP2(S272)
Akt-mTOR-p70S6K-PI3K	PLEC(S4406)
Akt-mTOR-p70S6K-PI3K	PLEC(T4411)
Akt-mTOR-p70S6K-PI3K	RBL2(S1138)
Akt-mTOR-p70S6K-PI3K	RBM14(S618)
Akt-mTOR-p70S6K-PI3K	RICTOR(T1135)
Akt-mTOR-p70S6K-PI3K	RPS6KB1(S427)
Akt-mTOR-p70S6K-PI3K	SART1(S448)
Akt-mTOR-p70S6K-PI3K	SETD1A(S1171)
Akt-mTOR-p70S6K-PI3K	SPATS2L(S135)
Akt-mTOR-p70S6K-PI3K	UCK1(S253)
Akt-mTOR-p70S6K-PI3K	WDHD1(S374)
Akt-mTOR-p70S6K-PI3K	YBX1(S209)
Akt-mTOR-p70S6K-PI3K	ZFP36L1(S334)
p70S6K-PI3K-PKC-ROCK	ZYX(S143)
Akt-CAMK2-EGFR	ATG4B(S383)
Akt-CAMK2-EGFR	DSP(T2612)
Akt-CAMK2-EGFR	FAM177A1(S70+T71)
Akt-CAMK2-EGFR	LSR(S643+S646)
Akt-CAMK2-EGFR	MAP7D1(S834)
Akt-CAMK2-EGFR	NCOR2(S1018)
Akt-CAMK2-EGFR	NOTCH2(S1804)
Akt-CAMK2-EGFR	PTGES3(S148)
Akt-CAMK2-EGFR	RANBP2(S2628)
Akt-CAMK2-EGFR	RANGAP1(S428+S442)
Akt-CAMK2-EGFR	ROCK2(S1134+S1137)
Akt-CAMK2-EGFR	SMARCAD1(S124+S127)
Akt-CAMK2-EGFR	SRRM2(S1398+S1404)
Akt-CAMK2-EGFR	TRMT112(S119)
Akt-CAMK2-EGFR	YWHAQ(S230)
Akt-CAMK2-ERK	GORASP2(T423+S451)

Akt-CAMK2-ERK	PRKCD(T507)
Akt-EGFR-ERK	AHNAK(S1298)
Akt-EGFR-ERK	MAP2K4(T391+S394)
Akt-EGFR-ERK	MAVS(S258)
Akt-EGFR-ERK	MCM3(S711+T722)
Akt-EGFR-MEK	RSF1(S1359+S1375)
Akt-ERK-MEK	PPP1R12A(T696)
Akt-mTOR-PI3K	AKT1S1(S183)
Akt-mTOR-PI3K	ARFGAP2(S368)
Akt-mTOR-PI3K	BAHD1(S121)
Akt-mTOR-PI3K	BCL7C(S126)
Akt-mTOR-PI3K	CCNL1(S335+S338)
Akt-mTOR-PI3K	CTTN(T440)
Akt-mTOR-PI3K	EEF2K(S71+S74)
Akt-mTOR-PI3K	EIF4EBP1(S65+T68)
Akt-mTOR-PI3K	EIF4EBP1(T37+T41)
Akt-mTOR-PI3K	EIF4EBP1(T68+T70)
Akt-mTOR-PI3K	EIF4EBP2(S65+T70)
Akt-mTOR-PI3K	EIF4EBP2(T70)
Akt-mTOR-PI3K	EIF4EBP2(Y34+T46)
Akt-mTOR-PI3K	FAM54A(S305)
Akt-mTOR-PI3K	FAM83H(S1024)
Akt-mTOR-PI3K	FOXK1(S249+S253)
Akt-mTOR-PI3K	FOXK1(S257)
Akt-mTOR-PI3K	FOXK2(S369)
Akt-mTOR-PI3K	FOXK2(S385)
Akt-mTOR-PI3K	GSK3B(S9)
Akt-mTOR-PI3K	LAMTOR1(S98)
Akt-mTOR-PI3K	LARP1(S1058)
Akt-mTOR-PI3K	LARP1(S774)
Akt-mTOR-PI3K	LIMA1(S230)
Akt-mTOR-PI3K	MYC(S62)
Akt-mTOR-PI3K	MYCBP2(S2833)
Akt-mTOR-PI3K	PCBP1(S246)
Akt-mTOR-PI3K	PCBP1(S262)
Akt-mTOR-PI3K	PCBP1(S263)
Akt-mTOR-PI3K	PDE3B(S494)
Akt-mTOR-PI3K	PUM1(S209)
Akt-mTOR-PI3K	RITA(S248)
Akt-mTOR-PI3K	RN3L1(S44)
Akt-mTOR-PI3K	RPS6KB1(S447+S452)
Akt-mTOR-PI3K	SEC14L1(T234)
Akt-mTOR-PI3K	SUN2(S20)
Akt-mTOR-PI3K	TBX2(S657)
Akt-mTOR-PI3K	TP53BP1(S1430)
Akt-mTOR-PI3K	TPR(T650)
Akt-mTOR-PI3K	UBA1(S816)
Akt-mTOR-PI3K	USP32(S1361)
Akt-mTOR-PI3K	USP32(S1366+S1371)
Akt-mTOR-PI3K	VWA7(S305+S325)
Akt-mTOR-PI3K	WDHD1(S374+S383)
Akt-mTOR-PI3K	ZNF185(S64)
EGFR-ERK-MEK	INCENP(T145+S148)
EGFR-PI3K-PKC	SPTBN1(S2358)
mTOR-p70S6K-PI3K	BOD1L1(S635)
mTOR-p70S6K-PI3K	BOD1L1(S637)
mTOR-p70S6K-PI3K	C14orf43(T698+S700+S718)
mTOR-p70S6K-PI3K	C5orf30(S167)
mTOR-p70S6K-PI3K	F12(S335+T337)
mTOR-p70S6K-PI3K	RBM14(S620)
mTOR-p70S6K-PI3K	WWTR1(S89)
p70S6K-PI3K-PKC	ZYX(S142)
Akt-CAMK2	ARHGAP35(S975+S985)
Akt-CAMK2	CACNB1(T217+S228+Y242)
Akt-CAMK2	CARHSP1(S30+S32+S41)
Akt-CAMK2	DDHD1(T726+S727)
Akt-CAMK2	EEF1B2(S106)
Akt-CAMK2	FAM122B(S222+S245)
Akt-CAMK2	FBXW7(S396)
Akt-CAMK2	FKBP15(S1114)
Akt-CAMK2	FOXO3(S75)
Akt-CAMK2	FSBP(S191+S193+T204)
Akt-CAMK2	GIT2(S418+S421)
Akt-CAMK2	GPKOW(S471)
Akt-CAMK2	INCENP(T239)
Akt-CAMK2	KIAA0284(S951+S954)
Akt-CAMK2	KIAA1429(S138)
Akt-CAMK2	KLHDC4(S413+S418)
Akt-CAMK2	MAP2K4(S257)
Akt-CAMK2	MARK4(T214)
Akt-CAMK2	MAVS(S152+T163)

Akt-CAMK2	MKL2(S207+T227)
Akt-CAMK2	NKX6-3(T8)
Akt-CAMK2	PARP4(T1119)
Akt-CAMK2	PRKACA(T198)
Akt-CAMK2	PRKACA(T202)
Akt-CAMK2	PRKCD(T511)
Akt-CAMK2	PRKCI(T410)
Akt-CAMK2	RAB11FIP2(S150)
Akt-CAMK2	RPUSD1(S271)
Akt-CAMK2	RRM2(S20)
Akt-CAMK2	SAP30BP(S18+S22)
Akt-CAMK2	SERHL2(T272)
Akt-CAMK2	SMN1(S28+S31)
Akt-CAMK2	STRN(S245)
Akt-CAMK2	TFG(S193+S197)
Akt-CAMK2	TOP2B(S1522+S1524)
Akt-CAMK2	TRIP12(S1317+S1322)
Akt-CAMK2	UBAP2L(S428)
Akt-CAMK2	UNC13D(S150)
Akt-CAMK2	WAPAL(S77)
Akt-EGFR	DCAF5(S648)
Akt-EGFR	EIF4G1(T205+T207)
Akt-EGFR	GAPVD1(S1105)
Akt-EGFR	KDM1A(T59)
Akt-EGFR	MFAP1(T267)
Akt-EGFR	PA2G4(S2+T11)
Akt-EGFR	PFDN4(S125)
Akt-EGFR	PXN(S126+S130)
Akt-EGFR	TNFRSF10A(S466)
Akt-ERK	AGAP2(S808)
Akt-mTOR	EP400(T1738)
Akt-mTOR	NSD1(S979)
Akt-mTOR	RAPGEF6(S1070)
Akt-mTOR	SERBP1(S392)
Akt-mTOR	UBA1(S816+S820)
Akt-p70S6K	BTF3(S161)
Akt-p70S6K	RAD18(S99)
Akt-PI3K	CCNL1(T325+S341+S342)
Akt-PI3K	CDC42EP2(S109)
Akt-PI3K	FOXK1(S236+S257)
Akt-PI3K	GAPVD1(S566+S569)
Akt-PI3K	SEMA4B(S825)
Akt-PI3K	STIP1(S16)
Akt-PKC	YEATS2(T1149+T1165)
CAMK2-EGFR	NUP153(S209)
CAMK2-EGFR	SCRIB(S1306+S1309)
CAMK2-EGFR	SPICE1(S760+S764)
CAMK2-EGFR	TRIM28(S43)
EGFR-ERK	C14orf43(S700+S709)
EGFR-MEK	MAPK1(T185+Y187)
EGFR-MEK	RANBP2(S1869)
EGFR-MEK	TPR(S2155)
EGFR-p70S6K	TMCC1(S382)
ERK-mTOR	C14orf43(S461)
ERK-p70S6K	RXRA(T23)
MEK-PKC	ERF(S532)
mTOR-p70S6K	USP5(S785)
mTOR-PI3K	ATRX(S594)
mTOR-PI3K	ATRX(S598)
mTOR-PI3K	BCAS3(S838)
mTOR-PI3K	CTTN(S438)
mTOR-PI3K	EEF2K(S74)
mTOR-PI3K	FOXK2(T389+S392)
mTOR-PI3K	HDGFRP2(S454)
mTOR-PI3K	IBTK(Y996+S1004)
mTOR-PI3K	LARP1(S1056)
mTOR-PI3K	LARP4B(S568)
mTOR-PI3K	LIMA1(S225)
mTOR-PI3K	MAF1(S60+S68)
mTOR-PI3K	MKI67IP(S218+T240)
mTOR-PI3K	MREG(S213)
mTOR-PI3K	NDRG3(S331)
mTOR-PI3K	PCBP1(S264)
mTOR-PI3K	PLEKHA3(S244)
mTOR-PI3K	PXN(S137)
mTOR-PI3K	PXN(T136)
mTOR-PI3K	SPHKAP(T741)
mTOR-PI3K	USP24(S2561)
mTOR-PI3K	USP24(T2565)
p70S6K-PI3K	AKAP11(S18)
p70S6K-PI3K	CD2AP(S234)

p70S6K-PI3K	CPSF7(T67+Y72+S75)
p70S6K-PI3K	FKBP15(S1012)
p70S6K-PI3K	FKBP15(S346)
p70S6K-PI3K	PFKFB2(S483)
p70S6K-PKC	EPS8L2(S459)
p70S6K-PKC	EPS8L2(S466)
p70S6K-PKC	OR1A1(T280+Y288)
p70S6K-PKC	TPD52(S176)
p70S6K-PKC	UBL7(S230)
p70S6K-PKC	YAP1(S61)
PI3K-PKC	KIAA1598(S249)
PI3K-PKC	NCBP1(S22)
PI3K-PKC	PAK2(S197)
PI3K-PKC	SCNN1D(S6)
PKC-ROCK	EMD(S173)
Akt	ACACA(S29)
Akt	AFTPH(S411)
Akt	AHNAK(S4360)
Akt	AHNAK(T4766)
Akt	AKAP13(S790)
Akt	ANK3(S1326+S1327+T1334)
Akt	ANLN(S661)
Akt	ARAP1(S229)
Akt	ASXL2(S834+S842)
Akt	ATF2(S90)
Akt	ATXN2L(S559)
Akt	B4GALT1(S9+S11+S18)
Akt	BAG3(S377+S386)
Akt	BAG3(S385)
Akt	BAIAP2L1(T416)
Akt	BANP(S90)
Akt	BPTF(S1060+T1064)
Akt	BRD9(S588)
Akt	BZW2(S412+S414)
Akt	C17orf85(S25)
Akt	CAMSAP2(S611)
Akt	CAMSAP3(S1048)
Akt	CAMSAP3(S1048+S1051)
Akt	CBL(S452)
Akt	CCDC43(T139)
Akt	CCDC6(S254)
Akt	CCDC6(T436)
Akt	CHAMP1(S282)
Akt	CIC(S77)
Akt	CIZ1(T872)
Akt	CLIP1(S152)
Akt	CLNS1A(S197)
Akt	CP(T528)
Akt	CSTF2(S524)
Akt	CTNND1(T177)
Akt	CTPS1(S574+S575)
Akt	CYP2S1(T295+T304+T314)
Akt	DAP(S51)
Akt	DAXX(S688+S702)
Akt	DCAF5(S531)
Akt	DCP1A(S180)
Akt	DCTPP1(T170)
Akt	DIDO1(S898)
Akt	DIP2A(T279)
Akt	DIP2B(S153)
Akt	DNMT1(S394)
Akt	DPF2(Y172)
Akt	DSP(S2821+S2825)
Akt	DYNC1LI1(S207)
Akt	EIF4G1(S204)
Akt	EIF4G1(T211)
Akt	EIF5B(S135+S137)
Akt	ERBB2IP(Y920+S932)
Akt	EXOC1(S501)
Akt	EXOSC9(S392+S394)
Akt	FAM102B(S320)
Akt	FGFR1OP(S160)
Akt	FKBP15(S311)
Akt	FKBP3(S152)
Akt	FLNA(S2163)
Akt	FTH1(S183)
Akt	FUBP1(S630)
Akt	FYTTD1(S23)
Akt	GAB2(T287)
Akt	GAPDH(T75)
Akt	GAPVD1(S569)

Akt	GAPVD1(S758+S761)
Akt	GATAD2B(S129+S135)
Akt	GEMIN5(S778)
Akt	GOLGB1(S17)
Akt	GORASP2(S451)
Akt	GRIPAP1(S692)
Akt	GSG2(S179)
Akt	GTF2I(S679)
Akt	GYS1(S727)
Akt	HCFC1(S1507)
Akt	HMGCS1(S495)
Akt	HNRNPK(S116)
Akt	INF2(S1149)
Akt	KDM2A(S718)
Akt	KDM2A(T713+S718+T720)
Akt	KIAA0284(S655)
Akt	KIAA1429(S133)
Akt	KIAA1522(S161+T162)
Akt	KIAA1731(S407+S411+T415)
Akt	KLHL20(S263+T270+S273)
Akt	KRT19(S10)
Akt	LAD1(S121+S123)
Akt	LARP4(S597)
Akt	LRIG1(S1044)
Akt	MACF1(S3927)
Akt	MAP4(S507+T521)
Akt	MCM3(S711)
Akt	MCRS1(S282)
Akt	MFF(T138)
Akt	MIIP(S303)
Akt	MKI67(S2471)
Akt	MKI67IP(T227)
Akt	MKI67IP(T234+T238)
Akt	MTMR3(S613)
Akt	MTMR4(S610)
Akt	MUC5AC(T2223+S2224+T2225)
Akt	MYL9(S20)
Akt	MYL9(T19+S20)
Akt	NACA(S166)
Akt	NAGK(S76)
Akt	NAP1L1(T39)
Akt	NCAPG(S1015)
Akt	NCOR2(S2057+S2065+S2068)
Akt	NRP1(S894)
Akt	NUCKS1(S19)
Akt	NUMA1(S1945)
Akt	NUMA1(T2106)
Akt	NUP153(S343)
Akt	OR6C65(T277+S278+Y288)
Akt	PAK2(S141)
Akt	PBRM1(S39)
Akt	PDIA6(S428)
Akt	PHF8(S857)
Akt	PHKA1(S868+T877+S884)
Akt	PHKA2(S1015)
Akt	PKN1(T774)
Akt	PKP3(S313+S314)
Akt	POGZ(S333)
Akt	PPP1R2(S87)
Akt	PREX1(S319)
Akt	PTGES3(S151)
Akt	PXN(S340)
Akt	RAB11FIP1(S501)
Akt	RAB11FIP5(S176)
Akt	RAB3IP(S288)
Akt	RABGEF1(Y601)
Akt	RABL6(S425+S427)
Akt	RAD21(S449)
Akt	RAD50(T690)
Akt	RAD9A(S277)
Akt	RAI1(S683)
Akt	RAI1(S924)
Akt	RALGAPA1(S773)
Akt	RALGAPA1(S797)
Akt	RANBP2(S2263+S2270)
Akt	RBBP6(S1277)
Akt	RFFL(S240)
Akt	RHBDL1(S193+S202+Y214)
Akt	RPL24(T83)
Akt	RPLP0(S304+S307)
Akt	RPLP0(S307)

Akt	RPRD2(S976)
Akt	RPS17L(S113)
Akt	RPS17L(S115)
Akt	RPS6KA1(S221)
Akt	RWDD2B(T175)
Akt	SAC3D1(S402)
Akt	SAP30(S131+S138)
Akt	SAP30BP(S52)
Akt	SCAF1(S239)
Akt	SCAF1(S453)
Akt	SCAF1(T994+S997)
Akt	SCFD1(S373)
Akt	SCNM1(S183)
Akt	SCRIB(S1348)
Akt	SEC16A(S414+T415+S417)
Akt	SF1(S80+S82)
Akt	SF3B1(S129+T142)
Akt	SF3B2(T780)
Akt	SGSM1(S67)
Akt	SH2D3A(S125)
Akt	SIPA1L1(S174)
Akt	SIPA1L1(Y206+T209)
Akt	SLC3A2(S134)
Akt	SMARCA5(S66)
Akt	SMEK1(S771)
Akt	SMEK2(S840)
Akt	SNAPIN(S133)
Akt	SON(S1556)
Akt	SOX6(T180+S183)
Akt	SRRM2(S1401+S1404)
Akt	SSR3(S11)
Akt	STK24(T184)
Akt	STRN3(S257)
Akt	STRN4(S276)
Akt	SYAP1(S267)
Akt	TAB2(S524)
Akt	TBC1D10B(S656+S661)
Akt	TBC1D22A(S132)
Akt	TCF3(S134+S139)
Akt	TDRD7(S859)
Akt	TEX15(S194+S195+Y210)
Akt	TFDP1(S23)
Akt	TNS3(S776)
Akt	TP53BP1(S294)
Akt	TSC2(S1798)
Akt	TWF1(S143)
Akt	U2AF2(T119+T124+S142)
Akt	UBAP2L(T425)
Akt	UNG(T60)
Akt	UPF1(S1107)
Akt	USP13(T122)
Akt	USP32(S1423)
Akt	USP5(T623)
Akt	VAMP4(S30)
Akt	VTI1B(S138)
Akt	WDHD1(S367)
Akt	YTHDF1(S291)
Akt	ZFC3H1(T823)
Akt	ZNF276(S599)
Akt	ZNHIT3(S80)
Akt	ZNRF1(S52+S53)
Akt	ZZEF1(S1518)
CAMK2	ARHGEF2(S151)
CAMK2	ARSI(Y263)
CAMK2	CAC1A(S2275+T2277)
CAMK2	CCDC86(S18+S21)
CAMK2	DNMT3A(S6+S7+T12)
CAMK2	HUWE1(S649)
CAMK2	JUND(S255+S259)
CAMK2	KCTD15(S35+S38)
CAMK2	MKI67IP(S230+T234+T238)
CAMK2	PPP1R11(T109)
CAMK2	PRKCD(S664)
CAMK2	PTGES3(S113)
CAMK2	RPRD2(S628)
CAMK2	RRM2(S377)
CAMK2	SCRIB(S1439)
CAMK2	SMEK1(S117+S126)
CAMK2	TRIM33(T1102+S1105)
EGFR	AHNAK(S5448)
EGFR	ARHGAP17(S625)

EGFR	EHMT2(S140)
EGFR	EIF4G1(S1092)
EGFR	FASN(T2204)
EGFR	GCFC1(S557+S558)
EGFR	GORASP2(T433)
EGFR	ITGB4(S1457)
EGFR	LSM14A(S178+S182)
EGFR	NSFL1C(S114)
EGFR	PDS5B(S1177)
EGFR	RIPK2(S363)
EGFR	SRRM1(S769+S775)
EGFR	SRRM2(S2118+S2121)
EGFR	TNRC6B(S1816)
EGFR	TOP2A(S1393)
EGFR	WNK2(S1862)
ERK	CEP128(S217)
MEK	AHCTF1(S1283)
MEK	BCL2L11(S77)
MEK	ERF(S327)
MEK	MAPK1(Y187)
MEK	MAPK3(Y204)
mTOR	ALKBH5(S361)
mTOR	ASAP2(S822)
mTOR	CASZ1(S741)
mTOR	DOS(S361)
mTOR	EIF4EBP1(S65)
mTOR	EIF4EBP1(T70)
mTOR	EIF4EBP1(Y34+T45)
mTOR	EIF4EBP2(T46)
mTOR	FA13B(S14)
mTOR	FOXK1(S441+S445)
mTOR	FOXK2(S428)
mTOR	HN1(S87+S88)
mTOR	KLF16(S224+S246)
mTOR	MKI67(S2223)
mTOR	MKI67(S2708)
mTOR	NDRG3(S333+S334)
mTOR	PHF2(S539)
mTOR	RPS10P5(S157)
mTOR	ULK1(S556)
mTOR	ULK1(S638)
mTOR	WIZ(S1146)
mTOR	ZFP106(S861)
p70S6K	CELSR1(S1320)
p70S6K	CIB3(T6+T9+Y16)
p70S6K	CLSPN(S1289)
p70S6K	ITLN2(S18)
p70S6K	KRT18(S34)
p70S6K	MAP6(S793)
p70S6K	MAP7(S365)
p70S6K	MED1(S953)
p70S6K	PPP1R10(S591)
p70S6K	PRKAG1(Y280+T284+T287)
p70S6K	RFX7(S1081)
p70S6K	RHBDF1(S51)
p70S6K	THRAP3(S682)
p70S6K	WBP11(S237)
p70S6K	WDHD1(S333)
p70S6K	ZNF217(S795)
PI3K	AHNAK(S570)
PI3K	DLG5(S1075)
PI3K	DOCK7(S2131)
PI3K	EHBP1L1(S310)
PI3K	FAM102B(S350)
PI3K	FAM21C(S288)
PI3K	FBP2(T13)
PI3K	FKBP15(S344+S356)
PI3K	FOXK2(S369+S373)
PI3K	GGT5(S474)
PI3K	KLC1(S524)
PI3K	LARP1(S824)
PI3K	MUC5B(T490)
PI3K	PACS1(S355)
PI3K	PAK2(S141+T154)
PI3K	PKP3(S313)
PI3K	PREX1(S1179)
PI3K	PREX1(S1182)
PI3K	PUM1(S75)
PI3K	SPAG9(S203+T217)
PI3K	STMN1(S16)
PI3K	ULK1(S623)

PKC	ABCF1(S140)
PKC	AHNAK(S5841)
PKC	ARFGAP1(T135)
PKC	CCDC88C(S1887)
PKC	CDC40(S45)
PKC	EIF4B(S442+S445)
PKC	EIF4B(S459)
PKC	GOLGA5(S116)
PKC	MAP2K2(S26)
PKC	MARK3(S419)
PKC	MARK3(T530)
PKC	MKI67(S713)
PKC	NAA10(S182)
PKC	NAV1(S17)
PKC	NFATC2IP(S366)
PKC	NOP58(S502+S514)
PKC	NPM1(S70)
PKC	NRBF2(S120)
PKC	NUP214(T1021)
PKC	OR5K4(T134)
PKC	PPP4R2(S224)
PKC	PVRL1(S422)
PKC	RANBP2(S1160)
PKC	SHANK1(S958)
PKC	SPTBN2(S2384)
PKC	TPT1(S46)
PKC	TRA2B(T201)
PKC	TWISTNB(S328)
PKC	YTHDC1(S424)
ROCK	AAK1(S637)
ROCK	AHNAK(S819)
ROCK	DIP2A(S94)
ROCK	DIP2B(S100)
ROCK	DIP2B(Y98)
ROCK	FBXW12(S286)
ROCK	IQSEC1(S180)
ROCK	MKI67(S1329)
ROCK	MKI67(S1937)
ROCK	MKI67(T1315)
ROCK	MPRIP(S1014)
ROCK	PPP1R12A(S445)
ROCK	PPP1R12A(S903)
ROCK	PPP1R13L(S134)
ROCK	SAPCD2(T219)
ROCK	SPECC1L(S887)
ROCK	SPTBN1(S2341)
ROCK	SVIL(T852)
ROCK	SVIL(Y850)
ROCK	WHSC2(S363)

Other Supporting Information Files

Dataset S1
Dataset S2
Dataset S3

Supplementary References

1. Casado P*, et al.* (2013) Kinase-substrate enrichment analysis provides insights into the heterogeneity of signaling pathway activation in leukemia cells. *Sci. Signal.* 6(268):rs6.
2. Montoya A, Beltran L, Casado P, Rodriguez-Prados JC, & Cutillas PR (2011) Characterization of a TiO(2) enrichment method for label-free quantitative phosphoproteomics. *Methods* 54(4):370-378.
3. Casado P & Cutillas PR (2011) A self-validating quantitative mass spectrometry method for assessing the accuracy of high-content phosphoproteomic experiments. *Mol. Cell. Proteomics* 10(1):M110 003079.
4. Cutillas PR & Vanhaesebroeck B (2007) Quantitative profile of five murine core proteomes using label-free functional proteomics. *Mol. Cell. Proteomics* 6(9):1560-1573.
5. Tsou CC*, et al.* (2010) IDEAL-Q, an automated tool for label-free quantitation analysis using an efficient peptide alignment approach and spectral data validation. *Mol. Cell. Proteomics* 9(1):131-144.
6. Mann B*, et al.* (2008) ProteinQuant Suite: a bundle of automated software tools for label-free quantitative proteomics. *Rapid Commun. Mass Spectrom.* 22(23):3823-3834.
7. Escher C*, et al.* (2012) Using iRT, a normalized retention time for more targeted measurement of peptides. *Proteomics* 12(8):1111-1121.
8. Bolstad BM, Irizarry RA, Astrand M, & Speed TP (2003) A comparison of normalization methods for high density oligonucleotide array data based on variance and bias. *Bioinformatics* 19(2):185-193.
9. Smyth GK (2004) Linear models and empirical bayes methods for assessing differential expression in microarray experiments. *Stat. Appl. Genet. Molec. Biol.* 3(1):Article3.
10. Smyth GK (2005) *Limma: linear models for microarray data* (Springer New York).
11. R Core Team (2013) R: A language and environment for statistical computing (R Foundation for Statistical Computing).
12. Wickham H (2009) *ggplot2: elegant graphics for data analysis* (Springer New York).
13. Warnes GR *et al.* (2013) *gplots: Various R programming tools for plotting data*.
14. Wickham H (2007) Reshaping data with the reshape package. *J. Stat. Softw.* 21(12):1-20.
15. Csardi G & Nepusz T (2006) The igraph software package for complex network research. *InterJournal* Complex Systems:1695.
16. Shannon P, *et al.* (2013) RCytoscape: tools for exploratory network analysis. *BMC Bioinformatics* 14:217.
17. Shannon P*, et al.* (2003) Cytoscape: a software environment for integrated models of biomolecular interaction networks. *Genome Res.* 13(11):2498-2504.
18. Gobbi A, *et al.* (2014) Fast randomization of large genomic datasets while preserving alteration counts. *Bioinformatics* 30(17):i617-623.
19. Kim SY & Volsky DJ (2005) PAGE: parametric analysis of gene set enrichment. *BMC Bioinformatics* 6:144.

20. Lindsley CW, *et al.* (2005) Allosteric Akt (PKB) inhibitors: discovery and SAR of isozyme selective inhibitors. *Bioorg. Med. Chem. Lett.* 15(3):761-764.
21. Rehan M, Beg MA, Parveen S, Damanhouri GA, & Zaher GF (2014) Computational insights into the inhibitory mechanism of human AKT1 by an orally active inhibitor, MK-2206. *PLoS ONE* 9(10):e109705.
22. Hirai H, *et al.* (2010) MK-2206, an allosteric Akt inhibitor, enhances the antitumor efficacy by standard chemotherapeutic agents or molecular targeted drugs in vitro and in vivo. *Mol. Cancer Ther.* 9(7):1956-1967.
23. Sumi M., *et al.* (1991) The newly synthesized selective Ca^{2+}/calmodulin dependent protein kinase-II inhibitor KN-93 reduces dopamine contents in PC12H cells. *Biochem. Biophys. Res. Commun.* 181(3):968-975.
24. Tokumitsu H, *et al.* (1990) KN-62, 1-*N*,*O*-bis(5-isoquinolinesulfonyl)-*N*-methyl-*L*-tyrosyl-4-phenylpiperazin E, a specific inhibitor of Ca^{2+}/calmodulin-dependent protein kinase-II. *J. Biol. Chem.* 265(8):4315-4320.
25. Fry DW, *et al.* (1998) Specific, irreversible inactivation of the epidermal growth factor receptor and erbB2, by a new class of tyrosine kinase inhibitor. *Proc. Natl. Acad. Sci. U.S.A.* 95(20):12022-12027.
26. Bos M, *et al.* (1997) PD153035, a tyrosine kinase inhibitor, prevents epidermal growth factor receptor activation and inhibits growth of cancer cells in a receptor number-dependent manner. *Clin. Cancer Res.* 3(11):2099-2106.
27. Hancock CN, *et al.* (2005) Identification of novel extracellular signal-regulated kinase docking domain inhibitors. *J. Med. Chem.* 48(14):4586-4595.
28. Ohori M, *et al.* (2005) Identification of a selective ERK inhibitor and structural determination of the inhibitor-ERK2 complex. *Biochem. Biophys. Res. Commun.* 336(1):357-363.
29. Gilmartin AG, *et al.* (2011) GSK1120212 (JTP-74057) Is an Inhibitor of MEK Activity and Activation with Favorable Pharmacokinetic Properties for Sustained In Vivo Pathway Inhibition. *Clin.Cancer Res.* 17(5):989-1000.
30. Roberts PJ & Der CJ (2007) Targeting the Raf-MEK-ERK mitogen-activated protein kinase cascade for the treatment of cancer. *Oncogene* 26(22):3291-3310.
31. Favata MF, *et al.* (1998) Identification of a novel inhibitor of mitogen-activated protein kinase kinase. *J. Biol. Chem.* 273(29):18623-18632 (1998).
32. Garcia-Martinez JM, *et al.* (2009) Ku-0063794 is a specific inhibitor of the mammalian target of rapamycin (mTOR). *Biochem. J.* 421(1):29-42.
33. Liu QS, *et al.* (2010) Discovery of 1-(4-(4-Propionylpiperazin-1-yl)-3-(trifluoromethyl)phenyl)-9-(quinolin- 3-yl)benzo h 1,6 naphthyridin-2(1H)-one as a Highly Potent, Selective Mammalian Target of Rapamycin (mTOR) Inhibitor for the Treatment of Cancer. *J. Med. Chem.* 53(19):7146-7155.
34. Pearce LR, *et al.* (2010) Characterization of PF-4708671, a novel and highly specific inhibitor of p70 ribosomal S6 kinase (S6K1). *Biochem. J.* 431(2):245-255.
35. Okuzumi T, *et al.* (2009) Inhibitor hijacking of Akt activation. *Nat. Chem. Biol.* 5(7):484-493.
36. Raynaud FI, *et al.* (2009) Biological properties of potent inhibitors of class I phosphatidylinositide 3-kinases: from PI-103 through PI-540, PI-620 to the oral agent GDC-0941. *Mol. Cancer Ther.* 8(7):1725-1738.
37. Miller TW, Rexer BN, Garrett JT, & Arteaga CL (2011) Mutations in the phosphatidylinositol 3-kinase pathway: role in tumor progression and therapeutic implications in breast cancer. *Breast Cancer Res.* 13(6):224.

38. Raynaud FI, *et al.* (2007) Pharmacologic characterization of a potent inhibitor of class I phosphatidylinositide 3-kinases. *Cancer Res.* 67(12):5840-5850.
39. Martinybaron G, *et al.* (1993) Selective inhibition of protein kinase C isozymes by the indolocarbazole Gö 6976. *J. Biol. Chem.* 268(13):9194-9197.
40. Toullec D, *et al.* (1991) The bisindolylmaleimide GF-109203X is a potent and selective inhibitor of protein kinase C. *J. Biol. Chem.* 266(24):15771-15781.
41. McCluskey A, Sim ATR, & Sakoff JA (2002) Serine-threonine protein phosphatase inhibitors: Development of potential therapeutic strategies. *J. Med. Chem.* 45(6):1151-1175.
42. Li YM & Casida JE (1992) Cantharidin-binding protein - identification as protein phosphatase-2A. Proc. Natl. Acad. Sci. U.S.A. 89(24):11867-11870.
43. Tamura M, *et al.* (2005) Development of specific Rho-kinase inhibitors and their clinical application. *Biochim. Biophys. Acta-Proteins and Proteomics* 1754(1-2):245-252.
44. Ishizaki T, *et al.* (2000) Pharmacological properties of Y-27632, a specific inhibitor of Rho-associated kinases. *Mol. Pharmacol.* 57(5):976-983.